

Critical microjets in collapsing cavities

By MICHAEL S. LONGUET-HIGGINS¹ AND HASAN OGUZ²

¹Institute for Nonlinear Science, University of California, San Diego, La Jolla,
California 92093-0402, USA

²Department of Mechanical Engineering, The Johns Hopkins University, Baltimore,
MD 21218, USA

(Received 11 July 1994 and in revised form 28 November 1994)

Inward microjets are commonly observed in collapsing cavities, but here we show that jets with exceptionally high velocities and accelerations occur in certain critical flows dividing jet formation from bubble pinch-off. An example of the phenomenon occurs in the family of flows which evolve from a certain class of initial conditions: the initial flow field is that due to a moving point sink within the cavity.

A numerical study of the critical flow shows that in the neighbourhood of microjet formation the flow is self-similar. The local accelerations, velocities and distances scale as $t^{\beta-2}$, $t^{\beta-1}$ and t^β respectively, where $\beta = 0.575$. The velocity potential is approximately a spherical harmonic of degree $\frac{1}{4}$.

1. Introduction

Since the suggestion by Kornfeld & Suvorov (1944) that the damage to solid walls from cavitation bubbles may be due to the impact of high-speed, inward-pointing jets involved in bubble collapse, many experimental and numerical studies have been carried out which amply confirm this phenomenon. For references to the literature see for example Blake, Taib & Doherty (1986). The occurrence of high-speed jets has also been observed in bubbles bursting at a water surface (Blanchard & Woodcock 1980), in axisymmetric standing waves on water (Longuet-Higgins 1983) and in steep, two-dimensional waves meeting a vertical wall (Cooke & Peregrine 1981).

The above examples indicate that the spontaneous formation of high-speed jets at a time-dependent free surface is a general phenomenon of some interest. However, most theoretical studies have been numerical and there are few analytical models. The Dirichlet hyperboloid suggested by Longuet-Higgins (1983) can model only a part of the flow. The two-dimensional generalizations of the Dirichlet hyperbola suggested by Longuet-Higgins (1993, 1994) depend on F. John's semi-Lagrangian representation in a complex plane (John 1953), and cannot easily be extended to axisymmetric motions.

However, though we cannot expect to find many exact solutions satisfying the nonlinear free-surface conditions for all times t , nevertheless we can hope to make progress by studying solutions in which the initial conditions say at time $t = 0$, are given in terms of simple analytic functions, involving only a few parameters. We can then follow the development of the flow by numerical time stepping, using a boundary-integral technique, and see how this development changes as we vary the parameters of the initial flow.

Such was the approach adopted in the present paper. As a promising model we considered first the flow around a cavity in which there was a moving point source (or sink). The motion of the source introduces an asymmetry into the initial pressure distribution. At the same time, by allowing the strength S of the source to vary with

time in a certain way (see §2 below) it was possible to arrange that the flow near a certain point on the bubble surface approximates the flow in a Dirichlet hyperboloid. Hence the development of a jet was expected. Moreover the surfaces of constant pressure were initially of almost spherical shape, and could plausibly be taken as the initial surface of the bubble.

As shown in §2, this leads to initial pressure contours given in polar coordinates ρ, θ , by

$$\rho^{-4} + 2\rho^{-2} \cos \theta + D\rho^{-1} = C, \quad (1.1)$$

where C and D are constants: C is proportional to the pressure while D is a basic parameter of the flow. The initial flow resembles a Dirichlet ellipsoid or hyperboloid according to whether $D > 2$ or $D < 2$.

The boundary-integral method used for time stepping the solution is described in §3. In §4 are shown the results for forward integrations, $t > 0$. These did indeed show re-entrant jets as expected. In some cases the particle accelerations were large, though always finite.

However, integration in the reverse direction ($t < 0$) gave an unexpected result. Jets were usually found to occur (after a time delay) on the opposite side of the bubble. Moreover for some values of the parameters (say $D = 1, C < 0.4$) a jet was not formed, but instead a small cavity, or bubble, was split off from the main cavity, as is sometimes observed experimentally, see Pumphrey & Crum (1988) and Medwin & Beaky (1991). The critical flow dividing jet formation from bubble split-off corresponded to $C \approx 0.4$. At this value of C the calculated values of the velocity and acceleration became extremely large, perhaps infinite.

A close examination of the critical flow, see §5, reveals that it is locally self-similar, the velocities and accelerations are proportional to negative powers of $(t - t_1)$ where t_1 is the critical instant. In §6 we see that the velocity potential is described approximately (but not exactly) by a spherical harmonic of degree $\nu = \frac{1}{4}$. A discussion follows in §7.

2. The moving sink

Consider a point sink of strength $4\pi S$ moving in a straight line with instantaneous velocity V , as in figure 1. Both S and V are in general functions of the time t . In a stationary frame of reference the instantaneous streamlines are all directed radially inwards towards S , with velocity potential

$$\phi = \frac{S}{r}, \quad \frac{\partial \phi}{\partial r} = -\frac{S}{r^2}, \quad (2.1)$$

as in figure 1(a), r being the radial distance. If we take a frame of reference moving with velocity V with the sink S lying on the z -axis at a distance $a(t)$ from the origin O , then the streamlines will appear as in figure 1(b), with a stagnation point at O provided that

$$S/a^2 = V. \quad (2.2)$$

The velocity potential will be given by

$$\phi = S[x^2 + y^2 + (z - a)^2]^{-1/2} - Vz. \quad (2.3)$$

In the neighbourhood of the origin O , this becomes

$$\phi = \frac{S}{a} \left[1 + \frac{1}{2a^2} (2z^2 - x^2 - y^2) \right] \quad (2.4)$$

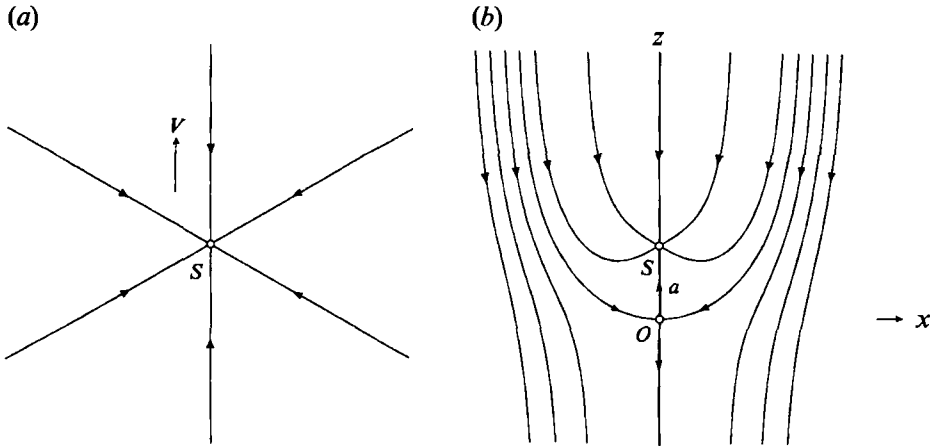


FIGURE 1. Instantaneous streamlines for a moving point sink in a reference frame which is (a) stationary, (b) moving with the sink.

neglecting terms of order $(z/a)^3$. Thus locally the flow has the form of a Dirichlet hyperboloid:

$$\phi = \frac{1}{4}A(2z^2 - x^2 - y^2) + f(t), \quad (2.5)$$

where

$$A = 2S/a^3, \quad f = S/a. \quad (2.6)$$

As the flow develops in time it will of course diverge from the Dirichlet hyperboloid. Nevertheless it would appear interesting to adopt the velocity potential (2.3) as an initial condition, with an appropriate free surface, and see what happens.

We first calculate the pressure field corresponding to equation (2.3). Writing

$$\rho \cos \vartheta = (z-a), \quad \rho \sin \vartheta = (x^2 + y^2)^{1/2} \quad (2.7)$$

and using the stationary frame of reference (figure 1a) we have

$$\phi = S/\rho, \quad \nabla\phi = -(S/\rho^3)(x, y, z-a), \quad \phi_t = \dot{S}/\rho + S\dot{a}(z-a)/\rho^3, \quad (2.8)$$

where a dot denotes d/dt . Since

$$-2p = (\nabla\phi)^2 + 2\phi_t + F(t) \quad (2.9)$$

we find

$$-2(p-p_\infty) = \frac{S^2}{\rho^4} + \left(\frac{2\dot{S}}{\rho} + 2S\dot{a} \frac{\cos \vartheta}{\rho^2} \right), \quad (2.10)$$

where p_∞ denotes the pressure at infinity. Now from (2.1) we have $S = a^2V$, and if the stagnation point 0 in figure 1(b) is to remain fixed momentarily, then $\dot{a} = V$. Hence

$$-2(p-p_\infty) = V^2 \left(\frac{a^4}{\rho^4} + 2 \frac{a^2}{\rho^2} \cos \vartheta + D \frac{a}{\rho} \right), \quad (2.11)$$

where

$$D = 2\dot{S}/(aV^2). \quad (2.12)$$

Writing $a/\rho = \kappa$ we see that the surfaces of constant pressure p are given by

$$\kappa^4 + 2\kappa^2 \cos \theta + D\kappa = C, \quad (2.13)$$

where C is a constant. We may take any of these surfaces as the free surface initially.

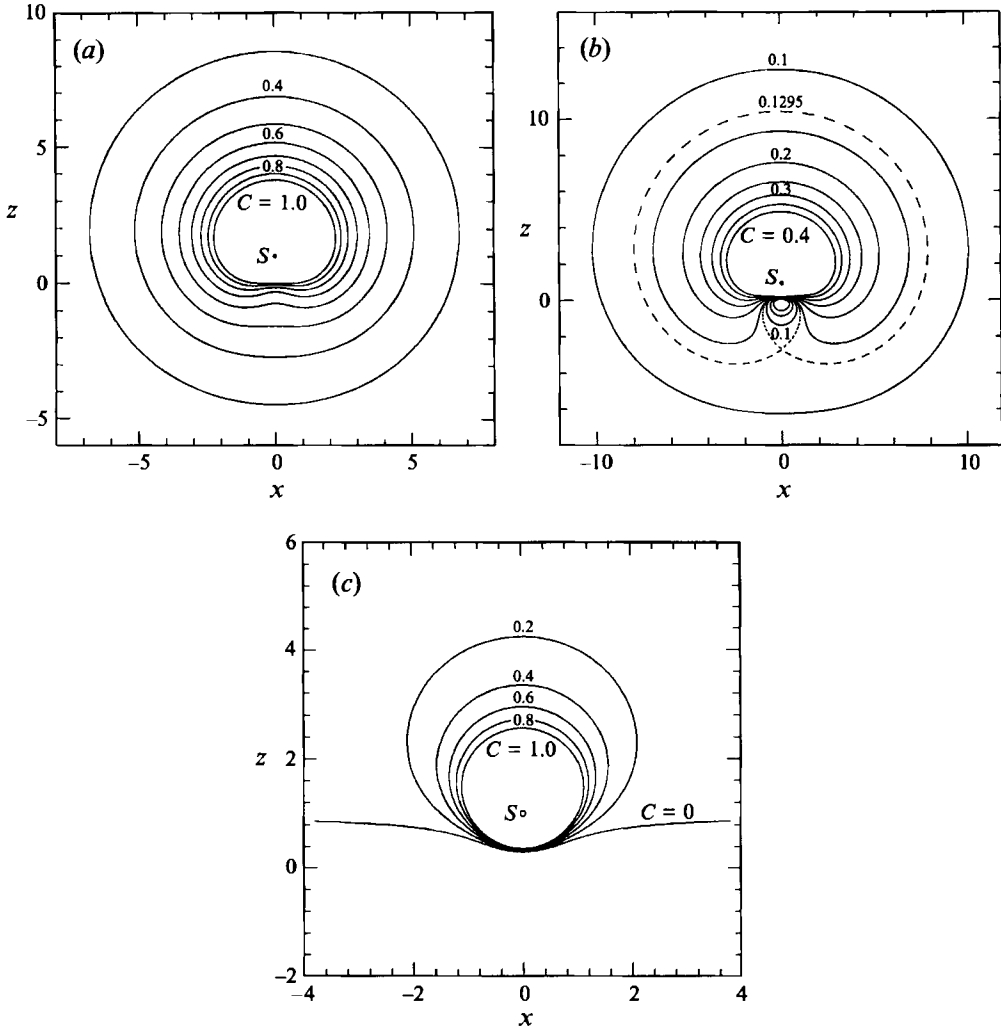


FIGURE 2. Contours of constant pressure for a moving point sink:
 (a) $D = 2$, (b) $D = 1$, (c) $D = 0$.

In Appendix A it is shown that we expect the initial flow to resemble a Dirichlet ellipsoid or hyperboloid according to whether

$$D \geq 2. \tag{2.14}$$

We shall be interested mainly in the case $D < 2$.

To determine the pressure contours, it is convenient to normalize the coordinates by setting $a = 1$. For given values of the constants C and D we may then solve equation (2.13) for κ as a function of ϑ . Since $\rho = 1/\kappa$ we may use ρ and ϑ as coordinates to plot the pressure contours.

The pressure contours in the cases $D = 2, 1$ and 0 are shown in figures 2(a), 2(b) and 2(c). In all cases the contours are very close together in the neighbourhood of the origin ($\rho = 1, \vartheta = \pi$), indicating a very high acceleration locally. In the case $D = 1$ (figure 2b) there is a pronounced pressure maximum on the axis at $\rho = 1.35, \theta = \pi$. Figure 2(c) is remarkable in that the innermost contour is almost exactly (but not quite) circular, as

may be verified by the reader from equation (2.11) with $D = 0$, $C = 1$. One contour has horizontal asymptotes, so the configuration may correspond approximately to a bubble approaching a free surface.

3. Time-stepping method

Given the initial shape of the bubble and the initial velocity potential

$$\phi = 1/\rho \quad (3.1)$$

on the bubble surface, we can integrate the motion by a boundary-integral method as follows. Because of the high accelerations and inertial forces we neglect gravity and surface tension. The time rate of change of ϕ following a particle is then given by

$$d\phi/dt = \frac{1}{2}(\nabla\phi)^2 + (p_\infty - p_B), \quad (3.2)$$

where p_∞ and p_B denote the pressure at infinity and at the bubble surface respectively; p_B is held constant. Note that initially $(p_\infty - p_B) = \frac{1}{2}CV^2$. Thus equation (3.2) gives $d\phi/dt$ on the bubble surface at time $t = t_0$ and hence ϕ on the new surface at time $t = t_0 + dt$. To find the normal component $\partial\phi/\partial n$ at time $(t_0 + dt)$ we solve the Dirichlet problem for ϕ using the boundary-integral method described by Oguz & Prosperetti (1993) for axisymmetric flows.

Typically, 40 surface points were used to discretize the bubble surface. Convergence tests were carried out with 80 surface points and no appreciable difference was noted as a result of higher resolution. After each step, surface points were uniformly distributed to reduce the instabilities commonly associated with the boundary-integral technique. In certain cases where sharp curvatures are formed it was necessary to use more points and achieve a high concentration of surface points near the regions of high curvature. In this case, the position of each point was assigned such that the arclength s_i at the i th point is

$$s_i = \left[\beta \left(\frac{i}{N} \right)^\gamma + (1 - \beta) \frac{i}{N} \right] L, \quad (3.3)$$

where L is the total arclength of the curve defining the bubble surface on the (R, Z) -plane. here β and γ are the distribution parameters. We set $\gamma = 3.5$ and $\beta = 0.5$ to obtain closely spaced points near the south pole of the bubble where $s = 0$. The modification to this procedure is trivial when high resolution is needed near the north pole.

A second-order-accurate Crank–Nicholson technique was used to step the solution in time. The implicitness of this procedure requires iteration at each time step. Convergence was assumed when the norm of the total correction was less than 0.01%. The number of iterations did not exceed ten in most cases. We used a variable time step in order to resolve the nearly singular behaviour of the flow and to reduce the computation time. Our past experience with the code (Oguz & Prosperetti 1993) led us to adopt the following formula for the time step:

$$\Delta t = \min \left[\frac{1}{2} \Delta s_{min}^2, \frac{3}{2} \Delta' t, \frac{0.05}{\max(|\nabla\phi|, d\phi/dt)} \right], \quad (3.4)$$

where Δs_{min} is the minimum segment length (minimum distance between two neighbouring points) and $\Delta' t$ is the previous time step.

In the absence of an external force, the total energy must be constant throughout the

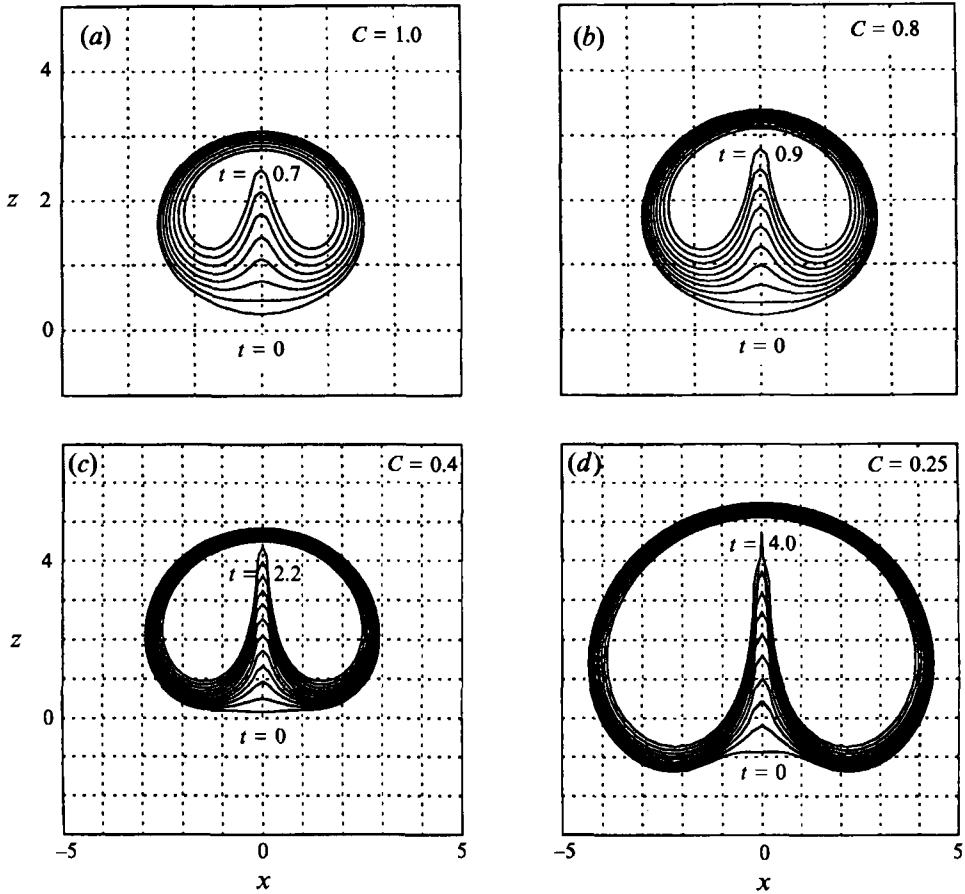


FIGURE 3. Successive profiles of the free surface in four cases when $D = 1$ and $t > 0$. Time interval between profiles: (a) 0.1, (b) 0.1, (c) 0.2, (d) 0.4.

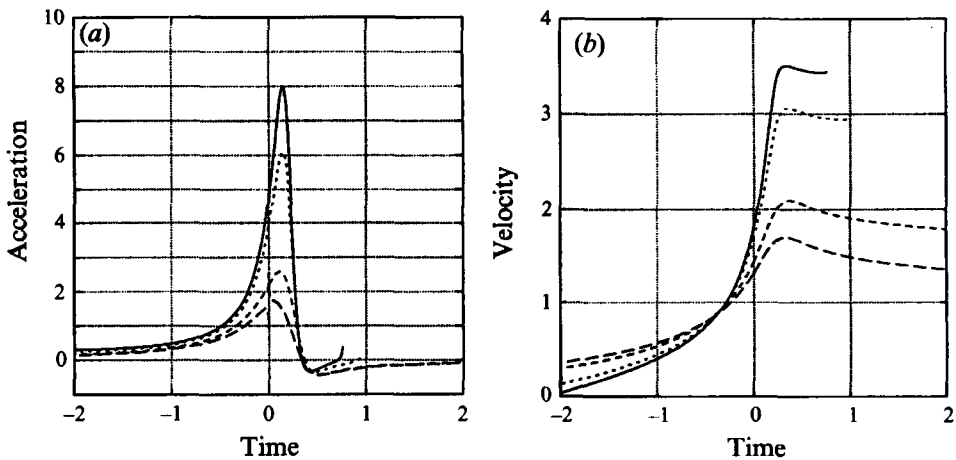


FIGURE 4. (a) Acceleration and (b) velocity of a surface particle on the axis of symmetry (south pole) when $D = 1$: —, $C = 1$; ····, 0.8; ----, 0.4; - · - ·, 0.25.

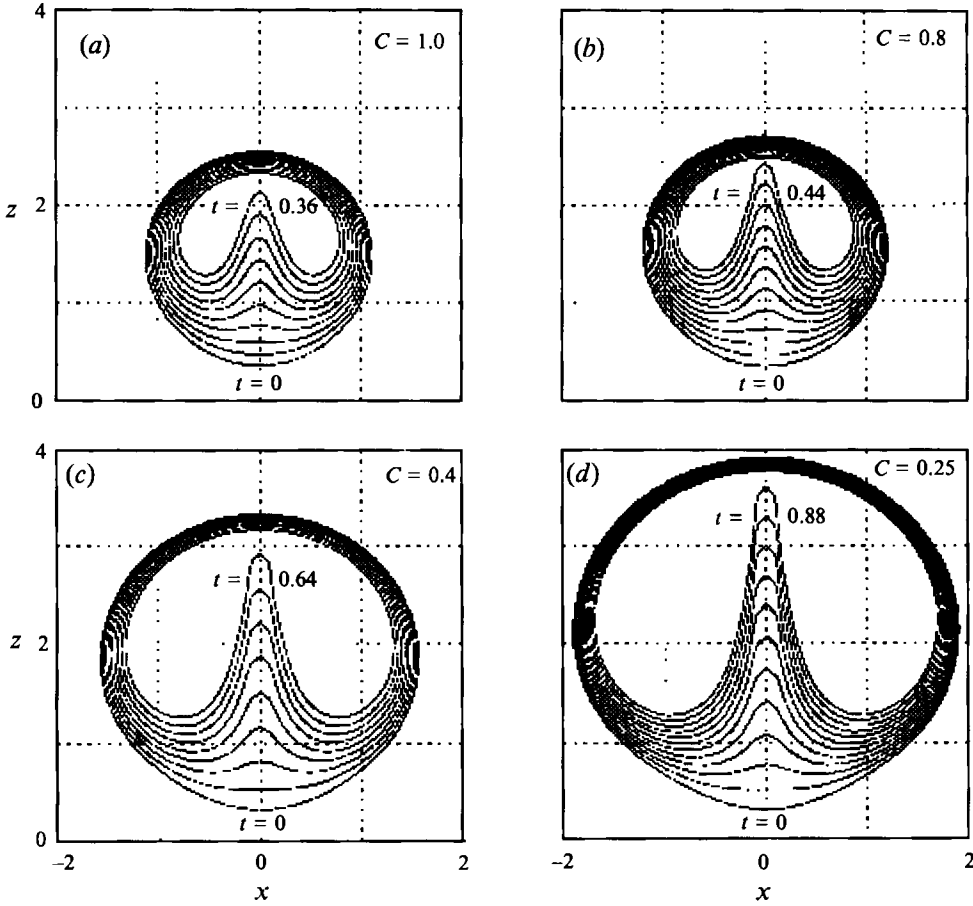


FIGURE 5. Successive profiles of the free surface in the case $D = 0$ when $t > 0$. Time interval between profiles: (a) 0.04, (b) 0.04, (c) 0.08, (d) 0.08.

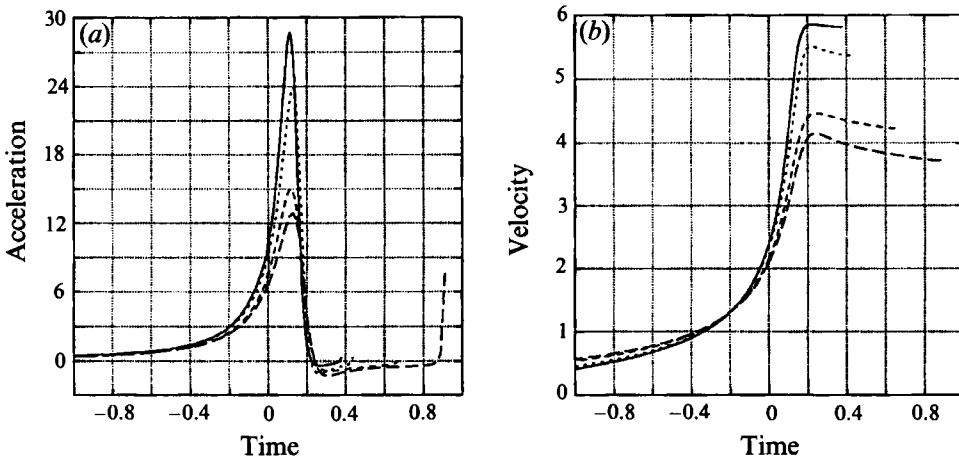


FIGURE 6. Acceleration and velocity of a surface particle on the axis of symmetry (south pole) when $D = 0$. For line styles see figure 4.

evolution of the flow. However, owing to regridding, discretization and time integration errors the total energy of the numerical simulations may deviate slightly from a constant. So a good test of accuracy is to monitor the total energy during the simulation. In all the reported cases in this paper, the total energy remained constant to better than 0.1% of the maximum kinetic energy of the system.

4. Results

The deformation of the free surface is shown in figure 3(a) for the typical case $D = 1.0$, $C = 1.0$. As expected, a re-entrant jet is formed, which rapidly approaches the opposite wall of the bubble. The corresponding acceleration and velocity of the tip of the jet, here called the 'south pole', is shown in figure 4 (solid lines). The acceleration peaks at the relatively high value 8 at around $t = 0.13$ then falls to slightly below zero as the jet 'coasts'. The velocity (figure 4b) rises to about 3.5 and then levels off. In the same diagram are shown the velocity and acceleration for other initial contours: $C = 0.8$, 0.4 and 0.25.

Figure 5 shows a similar set of surface profiles when $D = 0$ and $C = 1.0$, 0.8, 0.4 and 0.25. This time the accelerations are considerably higher, see figure 6(a). In the case $C = 1.0$, the tip acceleration peaks at nearly 28. The tip velocity rises to nearly 6. The velocities and accelerations at the 'north poles' ($\theta = 0$) are in these cases relatively small.

An interesting result is obtained if instead of integrating forwards we integrate backwards from $t = 0$, as may be done by reversing the sign of Δt . (Since there is no dissipation in the system, this is equivalent to considering a new problem in which the initial pressure and free surface are the same as before but the initial velocities are reversed. However in our notation we shall maintain the direction of time and speak of negative times t .)

From figure 8 it will be seen that at negative times, the values of the velocity and acceleration at the south poles remain small, but those at the north poles can be extremely high. From figure 7 we see there is now a re-entrant jet at the north poles, with particularly high acceleration and velocities in the case $C = 0.4$. In fact both the velocity and the acceleration become immeasurably high at around $t = -7.12$; see figure 8. In the case $C = 0.25$ a jet is not formed directly but a bubble appears to be pinched off instead. Indeed this was found for all values of C less than 0.4 (and with $D = 1$). As illustration we show in figure 9 the sequence of surface profiles and velocity vectors when $C = 0.35$ and 0.45. Thus $C = 0.4$ seems to be a critical value for this family of solutions when $D = 1.0$.

While these results suggest that the assumed flows could not exist as free flows over the entire time range $-\infty < t < \infty$, nevertheless they demonstrate two interesting phenomena:

(i) the possibility of a 'jet exchange' between two opposite poles of a nearly circular bubble;

(ii) the existence, in some families of flows, of critical cases characterized by jets with extremely high, possibly infinite, values of the acceleration and velocity. When a parameter lies on one side of the critical value the jets have finite acceleration and velocity. On the other side, a jet is not formed, but instead a bubble is pinched off.

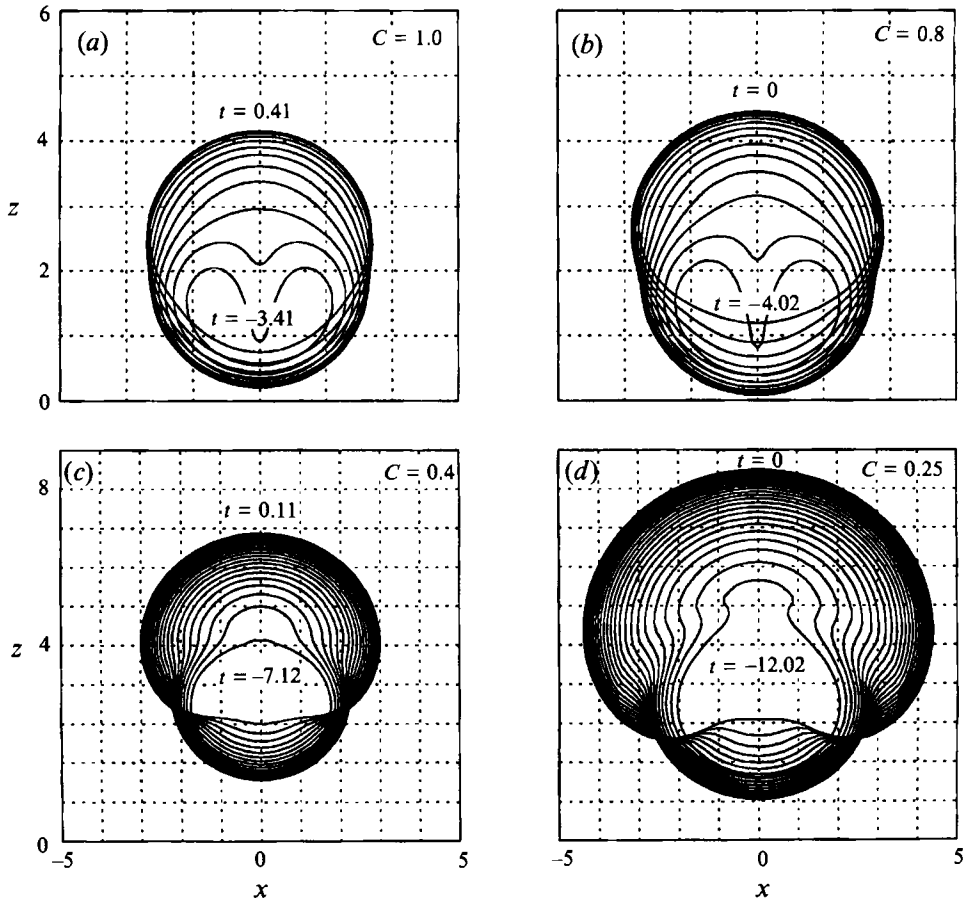


FIGURE 7. Successive profiles of the free surface in the case $D = 1$, $C = 1, 0.8, 0.4$ and 0.25 . Time interval between profiles: (a) 0.25, (b) 0.25, (c) 0.25, (d) 0.4.

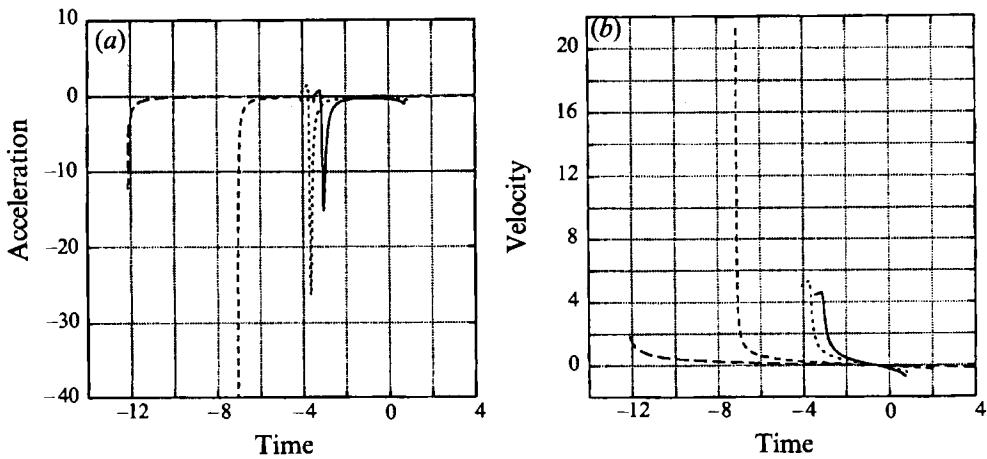


FIGURE 8. Acceleration and velocity of a particle at the north pole ($\theta = 0$) when $D = 1$. For line styles see figure 4.

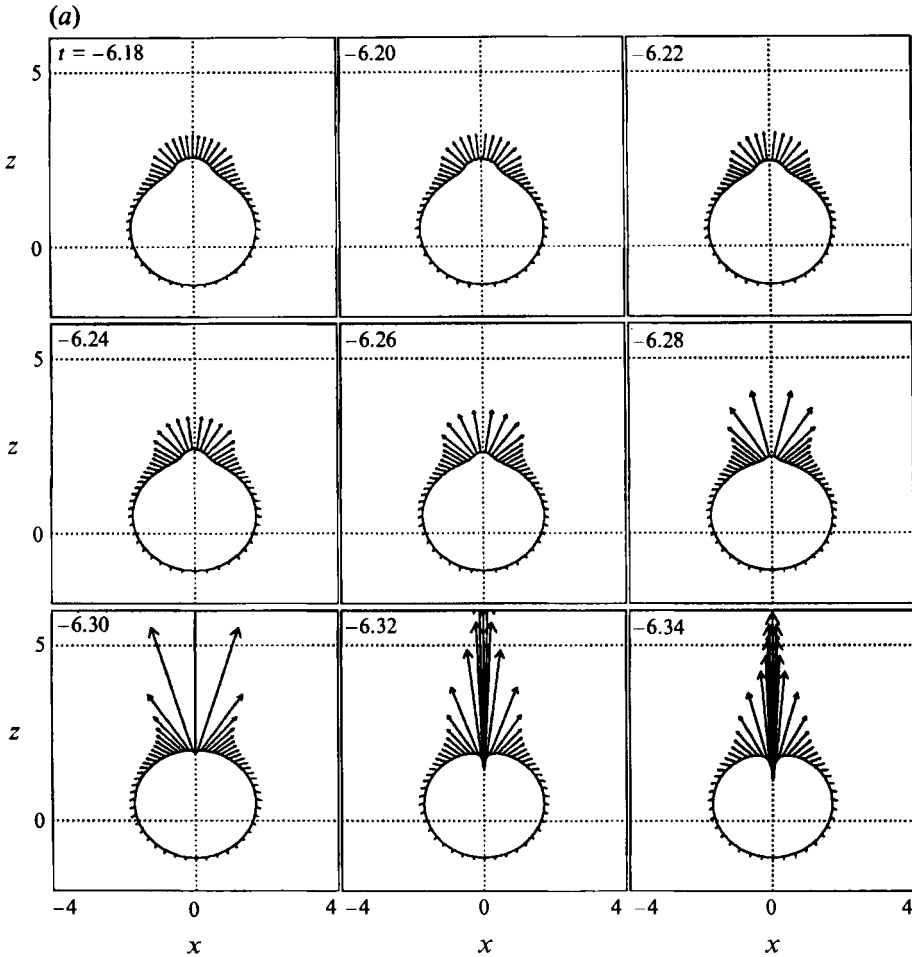


FIGURE 9(a). For caption see facing page.

5. The critical case

In this section we shall examine the critical flow for indications of self-similarity, in the case $D = 1$, $C = 0.4$.

Figure 8 has already indicated that the north-pole acceleration becomes large near a critical instant t_1 close to -7.12 . In figure 10 we show z_{tt} plotted against $(t - t_1)$ on a logarithmic scale, t_1 having been adjusted so as to give the best straight time fit to the plotted points. The result is that when $t_1 = -7.123$,

$$z_{tt} \propto (t - t_1)^{\beta-2}, \quad \beta = 0.575. \tag{5.1}$$

Integration of equation (5.1) yields for the velocity z_t of the tip of the jet

$$z_{tt} + B \propto (t - t_1)^{\beta-1}, \tag{5.2}$$

where B is a constant.

The value $B = 0.5$ gives the straight-line fit shown in figure 11. Thus the velocities at the tip are scaled like $(t - t_1)^{-0.425}$ approximately.

To examine the similarity of the profiles in space we have plotted in figure 12 both

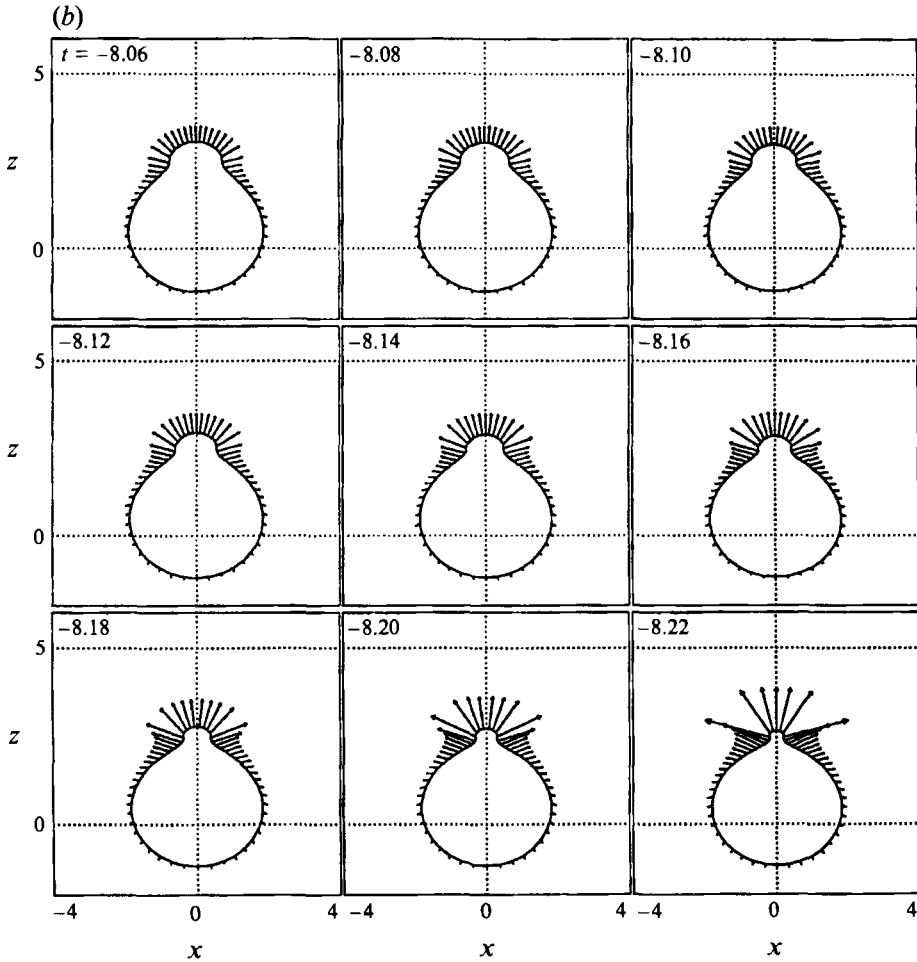


FIGURE 9. Profiles and velocity vectors at successive times $t < 0$ when $D = 1$. (a) $C = 0.45$, (b) $C = 0.35$. The velocity vectors are scaled $\times 0.25$. Note that if time were reversed, the velocity vectors would point inwards.

the profiles and the particle velocity vectors at six different times $t = -7.00, -7.02, \dots, -7.10$ on reduced scales as follows:

$$\left. \begin{aligned} \dot{\xi} &= (t - t_1)^{\beta-1} x_t, \\ \dot{\zeta} &= (t - t_1)^{\beta-1} (z_t + B) \end{aligned} \right\} \quad (5.3)$$

and

$$\left. \begin{aligned} \xi &= (t - t_1)^\beta x, \\ \zeta &= (t - t_1)^\beta (z_t + Bt + B'), \end{aligned} \right\} \quad (5.4)$$

where $B = 0.5, B' = -5.83$. In figure 13 these six profiles are superposed, and evidently there is a high degree of self-similarity.

6. The velocity field

Let us suppose that the velocity field in the neighbourhood of the north pole ($\theta = 0$) is given by a simple asymptotic expression valid as $t \rightarrow t_1$ on an inner scale δ which tends to 0 like $(t - t_1)^\beta$. Suppose further that when $x/\delta \rightarrow \infty$ this inner flow can be matched

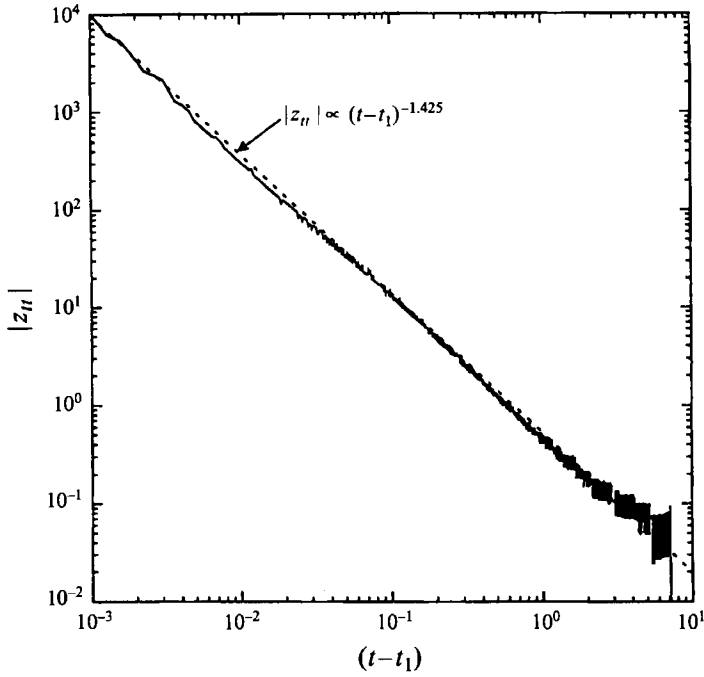


FIGURE 10. Logarithmic plot of the north-pole acceleration z_{tt} versus $(t-t_1)$ in the critical case $D = 1$, $C = 0.4$. Here $t_1 = -7.12$.

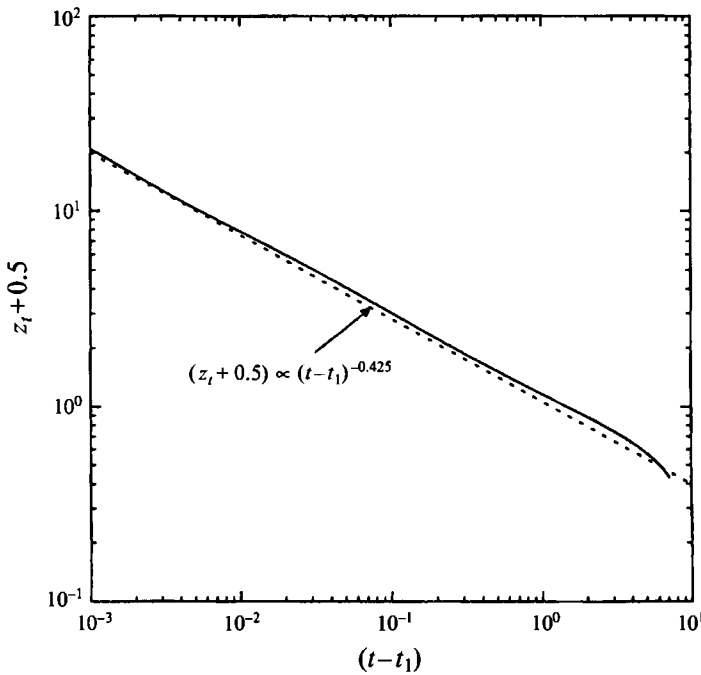


FIGURE 11. Logarithmic plot of $(z_t + B)$ versus $(t-t_1)$ where z_t is the north-pole velocity. Here $t_1 = -7.12$ and $B = 0.5$.

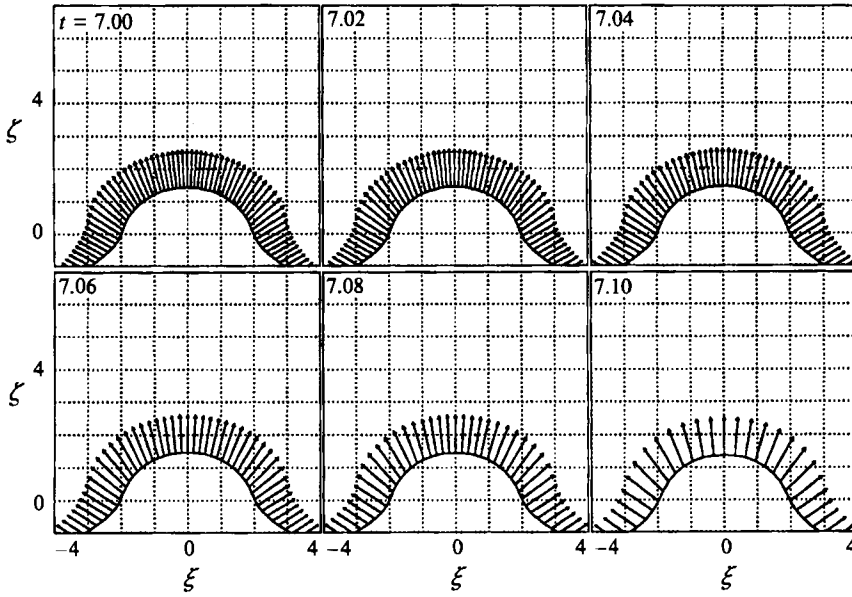


FIGURE 12. Surface profiles and velocity vectors scaled according to equations (5.3) and (5.4) when $D = 1$, $C = 0.4$.

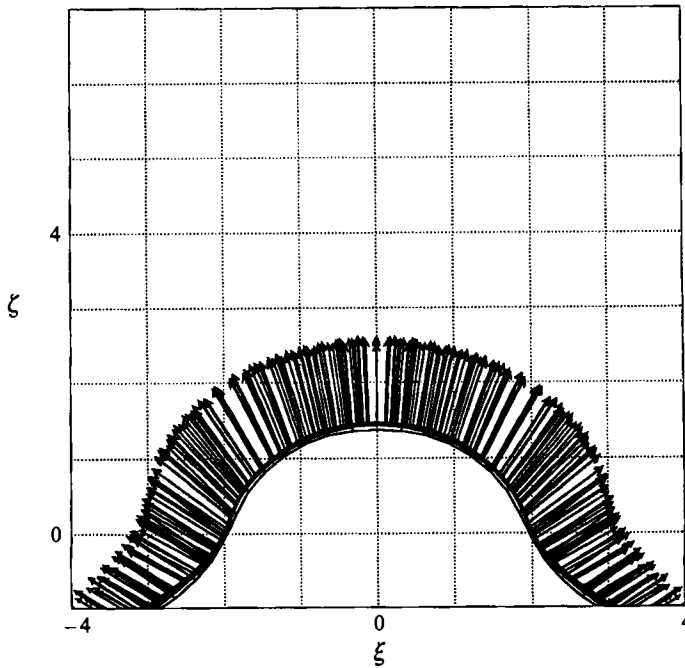


FIGURE 13. Superposition of the profiles and velocities in figure 12.

to the 'outer flow' in the rest of the cavity. To determine the behaviour of the inner flow for large values of x/δ we naturally inspect the surface profile at times t very close to t_1 .

Figure 14 shows an enlargement of the profile and velocity vectors when $t = -7.12$. There is a portion of the profile when $0.1 < x < 0.5$ which is relatively straight. Thus

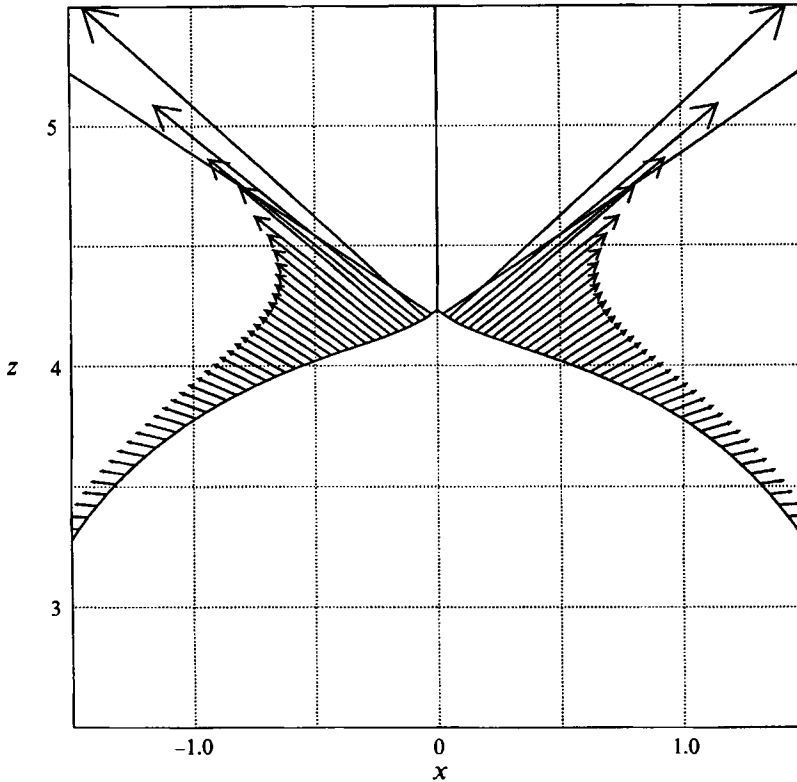


FIGURE 14. Surface profile (enlarged) and velocities (unscaled) in the critical case $D = 1$, $C = 0.4$ at $t = 7.12$. No scaling has been performed.

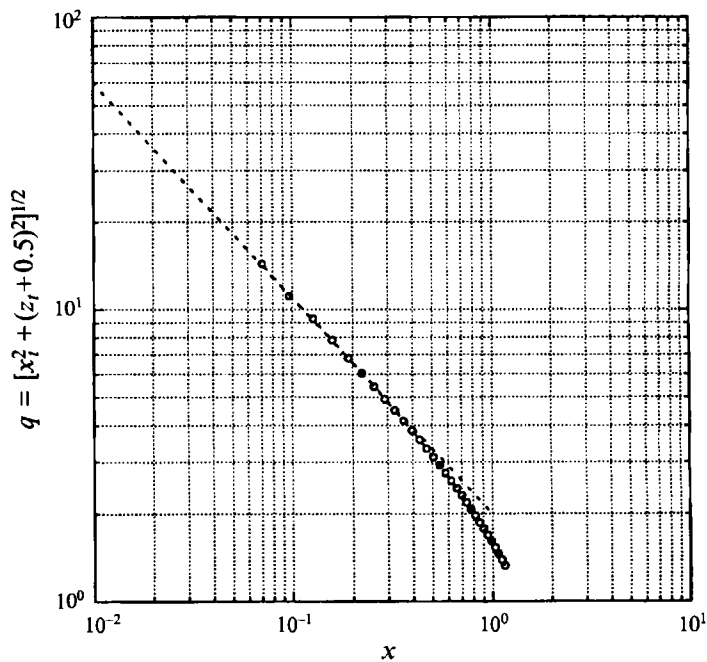


FIGURE 15. Logarithmic plot of the speed $q = [x_i^2 + (z_i + 0.5)^2]^{1/2}$ of a surface particle versus distance x from the axis of symmetry. The straight-line asymptote has slope -0.747 .

if we take (spherical) polar coordinates (r, θ) with the origin 0 lying on the axis of symmetry near (but not at) the north pole, then over the range of x indicated the coordinate θ will be nearly constant. So if we suppose that in this region the inner solution has the simple form

$$\phi \propto F(t) r^\nu P_\nu(\cos \theta), \tag{6.1}$$

where P_ν denotes a Legendre function of some unknown degree ν , the magnitude q of the velocity will vary as $r^{\nu-1}$. The appropriate value of ν may possibly be determined by examination of the velocity vectors in figure 14 as follows.

In figure 15 we have plotted the magnitude q of the reduced velocity, that is

$$q = [x_t^2 + (z_t + 0.5)^2]^{1/2}, \tag{6.2}$$

against the distance $x = r \sin \theta$ (6.3)

from the axis of symmetry. It will be seen that over the range $0.1 < x < 0.5$ the velocity q does indeed follow the power law

$$q \propto x^\gamma, \quad \gamma = -0.747 \tag{6.4}$$

indicated by the straight line. Thus it appears reasonable to take

$$\nu = \gamma + 1 = 0.253 \tag{6.5}$$

or $\nu = \frac{1}{4}$ approximately.

Note that for non-integral values of ν the Legendre function $P_\nu(\cos \theta)$ is analytic in $0 \leq \theta < \pi$, but with a logarithmic singularity at $\theta = \pi$ which need not concern us, since the potential (6.1) need only be valid in a region $|\theta| \leq \theta_c$ where $\theta_c < \pi$. From figure 14 θ_c is about 120° .

7. Analytic expressions

Combining the results of §§5 and 6 we have for the inner flow a velocity potential of the form

$$\phi = -S t^\lambda r^\nu P_\nu(\cos \theta), \tag{7.1}$$

where S , λ and ν are constants. (Here t stands for $t - t_1$.) To determine λ note that when $\theta = \text{constant} = 0$, say, then

$$\phi \propto t^\lambda r^\nu \tag{7.2}$$

and so $dr/dt = \phi_r \propto t^\lambda r^{\nu-1}$ (7.3)

or $r^{1-\nu} dr \propto t^\lambda dt$. (7.4)

Hence $r^{2-\nu} \propto t^{\lambda+1}$ (7.5)

provided $\nu \neq 2$. Therefore $r \propto t^\beta$ as in §5, where

$$\beta = (\lambda + 1)/(2 - \nu) \tag{7.6}$$

that is $\lambda = (2 - \nu)\beta - 1$. (7.7)

In §5, β was found to be 0.575 approximately. This yields $\lambda = 0.005$, which is small, perhaps not significantly different from zero.

The components of fluid velocity corresponding to equation (7.1) are

$$\left. \begin{aligned} \phi_r &= -S t^\lambda r^{\nu-1} \nu P_\nu(\mu), \\ \frac{1}{2} \phi_\theta &= -S t^\lambda r^{\nu-1} (1 - \mu^2)^{1/2} P'_\nu(\mu), \end{aligned} \right\} \tag{7.8}$$

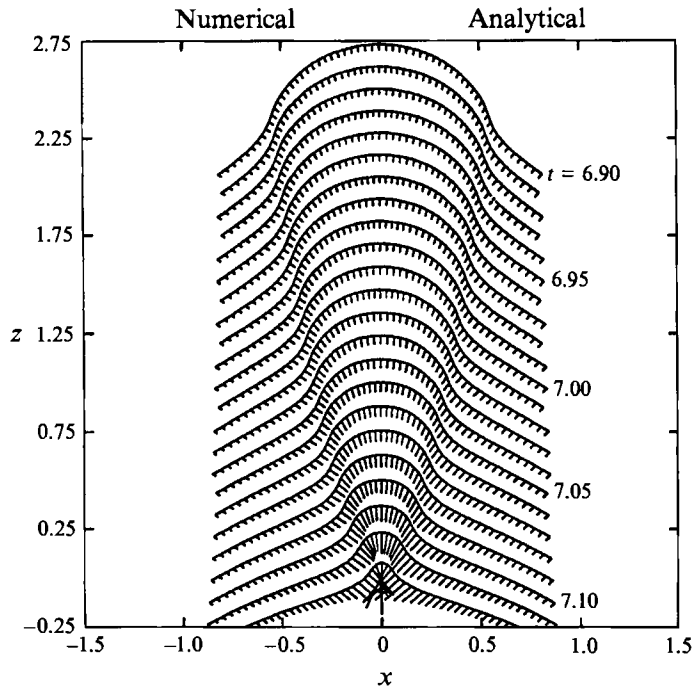


FIGURE 16. Comparison of the numerical profiles and velocity vectors with those given by the analytical expression (6.1).

where $\mu = \cos \theta$ and P'_v denotes $dP_v/d\mu$. In figure 16 these expressions are compared with the numerically calculated vectors, and it will be seen that the agreement is fairly good over the range $0 < x < 0.5$. The origin $r = 0$ was taken at the point $(\xi, \eta) = (2.23, 0)$.

8. Discussion

We have found numerically a family of jet-like flows, with analytic initial conditions, in which the velocity and acceleration may become exceedingly large near a certain instant $t = t_1$. The flows are described by a parameter C such that when C takes a critical value C_0 the velocities and accelerations at $t = t_1$ are infinite. When $C < C_0$, instead of a simple jet being formed a small bubble is split off from the main cavity. The velocities and accelerations are still high, however. A similar phenomenon appears in other types of flow, for example in the cavity resulting from impact of raindrops on a water surface, which was studied experimentally by Pumphrey & Crum (1988) and theoretically by Oguz & Prosperetti (1989); see also Longuet-Higgins (1990). Thus we may regard the present behaviour as generic. The advantage of the present family of flows is that the initial conditions are very simple, and given in terms of analytic functions.

We have studied the behaviour of the critical flow corresponding to $C = C_0$ and shown that it is locally self-similar and described by equation (7.1) approximately, though not exactly; see Appendix B. We may reasonably expect an exact 'inner solution' to exist, which could be matched asymptotically to the flow in the rest of the cavity. Moreover in neighbouring flows, when C is close to but not equal to C_0 we

might expect a more general type of asymptotic solution in which the accelerations are high but never infinite. The construction of such asymptotic flows and the study of the class of initial conditions which give rise to them would help towards a general understanding of jet formation, including the less violent south-pole jets seen in figures 4 and 6.

Appendix A. Proof of (2.12)

From equation (2.1) it follows that

$$D = \frac{2\dot{S}}{aV^2} = \frac{2\dot{S}/S}{V/a} = \frac{2\dot{S}/S}{\dot{a}} \quad (\text{A } 1)$$

since $V = \dot{a}$. Now for a Dirichlet ellipsoid the function $A(t)$ of equation (2.4) is given by

$$A = \dot{\alpha}/\alpha, \quad (\text{A } 2)$$

where $\alpha(t)$ satisfies
$$\dot{\alpha}^2(1 + L^3/\alpha^3) = U^2 \quad (\text{A } 3)$$

and L and U are positive constants. (For the hyperboloid, $L < 0$, see Longuet-Higgins 1978.) Now since $S = a^2V = a^2\dot{a}$ it follows from (2.5) that

$$A = 2S/a^3 = 2\dot{a}/a. \quad (\text{A } 4)$$

Comparing (A 2) and (A 4) we see that

$$\alpha = \kappa^2 a^2, \quad (\text{A } 5)$$

where κ is some constant. Therefore

$$S = a^2\dot{a} = \alpha^{1/2}\dot{\alpha}/\kappa^3 \quad (\text{A } 6)$$

and on differentiating logarithmically

$$\dot{S}/S = (\dot{\alpha}/2\alpha) + (\ddot{\alpha}/\dot{\alpha}). \quad (\text{A } 7)$$

But from equation (A 3) we find similarly

$$2\ddot{\alpha}/\dot{\alpha} = (3\dot{\alpha}/\alpha)L^3/(L^3 + \alpha^3). \quad (\text{A } 8)$$

Hence
$$\dot{S}/S = (\dot{\alpha}/2\alpha)[1 + 3L^3/(L^3 + \alpha^3)] = (\dot{a}/a)(1 + \frac{1}{2}E), \quad (\text{A } 9)$$

where
$$E = 6L^3/(L^3 + \kappa^6 a^6). \quad (\text{A } 10)$$

Thus from (A 1) and (A 9) we have

$$D = \frac{2\dot{S}/S}{\dot{a}/a} = 2 + E. \quad (\text{A } 11)$$

Since by (A 10) E has the same sign as L , this proves (2.12).

Appendix B. Boundary conditions for the flow (7.1)

If we neglect gravity and surface tension, the pressure p at the boundary is given by

$$-p = \phi_t + \frac{1}{2}(\nabla\phi)^2 + f(t). \quad (\text{B } 1)$$

Now from (6.1) and (6.10) we have

$$\left. \begin{aligned} \phi_t &= S\lambda t^{\lambda-1} r^\nu P_\nu, \\ (\nabla\phi)^2 &= S^2 t^{2\lambda} r^{2(\nu-1)} [(\nu P_\nu)^2 + (1-\mu^2) P_\nu'^2], \end{aligned} \right\} \quad (\text{B } 2)$$

where $\mu = \cos\theta$. If we introduce the scaled variable

$$R = r/t^\beta, \quad (\text{B } 3)$$

where β is given by (6.6), we find that the boundary condition $p = 0$ reduces to

$$\lambda S R^\nu P_\nu + \frac{1}{2} S^2 R^{2(\nu-1)} [(\nu P_\nu)^2 + (1-\mu^2) P_\nu'^2] + f^* = 0, \quad (\text{B } 4)$$

where $f^* = t^{2(1-\beta)} f(t)$. Since the other terms in equation (B 4) are independent of t by hypothesis we must have

$$f^* = \text{constant}, \quad f(t) \propto t^{2(\beta-1)}. \quad (\text{B } 5)$$

So taking $S = 1$ without loss of generality we may take the equation of the boundary as

$$H(R, \theta) = 0, \quad (\text{B } 6)$$

where

$$H(R, \theta) \equiv \lambda R^\nu P_\nu + \frac{1}{2} R^{2\nu-2} [(\nu P_\nu)^2 + (1-\mu^2) P_\nu'^2]. \quad (\text{B } 7)$$

The kinetic boundary condition can now be expressed in the form

$$DH/Dt = 0, \quad (\text{B } 8)$$

where

$$\frac{D}{Dt} = \frac{\partial}{\partial t} + \phi_r \frac{\partial}{\partial r} + \frac{1}{r} \phi_\theta \frac{1}{r} \frac{\partial}{\partial \theta} \quad (\text{B } 9)$$

and

$$\left. \begin{aligned} \frac{\partial}{\partial t} &= R_t \frac{\partial}{\partial R} = -\frac{\beta}{t} R \frac{\partial}{\partial R}, \\ \frac{\partial}{\partial r} &= R_r \frac{\partial}{\partial R} = t^{-\beta} \frac{\partial}{\partial R}, \\ \frac{\partial}{\partial \theta} &= -(1-\mu^2)^{1/2} \frac{\partial}{\partial \mu}. \end{aligned} \right\} \quad (\text{B } 10)$$

So equation (B 8) becomes

$$(\beta R + \nu R^{\nu-1} P_\nu) (\partial H / \partial R) + R^{\nu-2} (1-\mu^2) P_\nu' (\partial H / \partial \mu) = 0. \quad (\text{B } 11)$$

After substituting for H from (B 6) we obtain

$$[\nu P_\nu X - (\lambda + 1)] [(\nu - 1) W X + \lambda \nu P_\nu] + (1 - \mu^2) P_\nu' X [\frac{1}{2} W' X + \lambda P_\nu'] = 0, \quad (\text{B } 12)$$

where we have written

$$W = \frac{1}{2} [(\nu P_\nu)^2 + (1 - \mu^2) P_\nu'^2], \quad X = R^{\nu-2} \quad (\text{B } 13)$$

and we have used equation (6.7). This is our second boundary condition.

Now equation (B 7) can be written

$$\lambda P_\nu + W X + C X^{\nu/(2-\nu)} = 0. \quad (\text{B } 14)$$

If C vanishes, both conditions (B 12) and (B 14) become linear in X . They can both be satisfied simultaneously at all points on the free surface only if

$$2\lambda P_\nu [\nu(\nu-2) P_\nu W + (1-\mu^2) P_\nu' W'] \equiv W [\beta(\nu-2) W + 2\lambda(1-\mu^2) P_\nu'] \quad (\text{B } 15)$$

identically in μ . It can be verified that this is not generally true.

REFERENCES

- BLAKE, J. R., TAIT, B. B. & DOHERTY, G. 1987 Transient cavities near boundaries. Part 1. Rigid boundary. *J. Fluid Mech.* **170**, 479–497.
- BLANCHARD, D. C. & WOODCOCK, A. H. 1980 The production, concentration and vertical distribution of the sea-salt aerosol. *Ann. N.Y. Acad. Sci.* **338**, 330–347.
- COOKER, M. J. & PEREGRINE, D. H. 1991 Violent motion as near-breaking waves meet a wall. In *Breaking Waves, Proc. IUTAM Symp. Sydney, Australia* (ed. M. L. Banner & R. H. J. Grimshaw), pp. 291–297. Springer, 387 pp.
- JOHN, F. 1953 Two-dimensional potential flows with a free boundary. *Commun. Pure Appl. Maths* **6**, 497–503.
- KORNFELD, M. & SUVOROV, L. 1944 On the destructive action of cavitation. *J. Appl. Phys.* **15**, 495–506.
- LONGUET-HIGGINS, M. S. 1983 Bubbles, breaking waves and hyperbolic jets at a free surface. *J. Fluid Mech.* **127**, 103–121.
- LONGUET-HIGGINS, M. S. 1990 An analytical model of sound production by raindrops. *J. Fluid Mech.* **214**, 395–410.
- LONGUET-HIGGINS, M. S. 1993 Highly-accelerated, free-surface flows. *J. Fluid Mech.* **248**, 449–475.
- LONGUET-HIGGINS, M. S. 1994 Inertial shocks in surface waves and collapsing bubbles. *Proc. IUTAM Symp. on Bubble Dynamics and Interface Phenomena, Birmingham, UK, 6–9 Sep. 1993*.
- MEDWIN, H. & BEAKY, M. M. 1989 Bubble sources of the Knudsen and sea noise spectra. *J. Acoust. Soc. Am.* **86**, 1124–1130.
- OGUZ, H. N. & PROSPERETTI, A. 1993 Dynamics of bubble growth and detachment from a needle. *J. Fluid Mech.* **257**, 111–145.
- PROSPERETTI, A., CRUM, L. S. & PUMPHREY, H. C. 1989 The underwater noise of rain. *J. Geophys. Res.* **94**, 3255–3259.
- PUMPHREY, H. C. & CRUM, L. A. 1988 Acoustic emissions associated with drop impacts. In *Sea Surface Sound* (ed. B. R. Kerman), pp. 463–483. Dordrecht: Reidel, 639 pp.